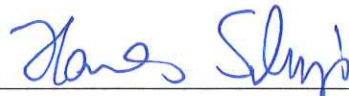


Mechanics of a Bio-Inspired One-Dimensional Thin-Film Mechanical Metamaterial

A thesis submitted in partial fulfillment of the requirement
for the degree of Bachelor of Science in
Physics from the College of William and Mary in Virginia,

by

Benjamin H. Skopic



Advisor: Prof. Hannes C. Schniepp



Prof. Seth Aubin

Williamsburg, Virginia
May 2019

Contents

Acknowledgments	ii
List of Figures	v
Abstract	v
1 Introduction	1
2 Theory	5
2.1 Thin-Films	5
2.2 Sacrificial Bonds	8
2.2.1 Peeling Delamination Mode	8
2.2.2 Lap Shear Joint Delamination Mode	11
2.3 Strain-Cycling	15
3 Experimental Technique	17
3.1 Imaging	17
3.2 Preliminary Tensile Test	19
3.3 High Precision Tensile Test	21
4 Results	23
5 Conclusion	32

Acknowledgments

I would like to thank Dr. Schniepp's Nanomaterials & Imaging lab for being welcoming to me over the past year and a half. Doctoral candidates Qijue Wang, Dinidu Perera, and Mahmoud Amin have been exceptionally helpful in mentoring me through my research. I look forward to formally joining the research team in the fall. I would also like to thank Olga Trofimova and the William and Mary Applied Research Center for teaching and allowing me to use their equipment such as the Phenom SEMs and the Hitachi FE-SEM. Finally, I want to thank Dr. David Kranbuehl from the Chemistry Department for granting me access to the rheometer.

List of Figures

1.1	Characterization of <i>Loxosceles</i> silk morphology	2
1.2	Single <i>Loxosceles</i> loop and loop junction	4
2.1	7k x magnification of <i>Loxosceles</i> silk	5
2.2	<i>Kendall 1975</i> model for thin-film peeling	7
2.3	Geometry of peeling failure mode	9
2.4	Plot of peeling geometry equations	11
2.5	<i>Kim 2006</i> single lap-joint failure mode	12
2.6	<i>Eriten 2011</i> contact model of rough surfaces	12
2.7	<i>Koebly 2017</i> stress-strain curve of strain-cycling	16
3.1	Sputter coater, FE-SEM, and rheometer	18
3.2	Examining the change in the <i>Loxosceles</i> loops throughout imaging . .	19
3.3	Experimental Setup for Preliminary and High Precision Tensile Tests	20
4.1	Plot and fit to determine surface energy	24
4.2	Combination of imaging statistics, mathematical modeling, and pre- liminary tensile test data	24
4.3	Sample rheometry trial	26
4.4	Comparison of preliminary tensile test and high precision tensile tests	28
4.5	AFM image of the surface of <i>Loxosceles</i> silk and Scotch®Tape	30
4.6	Profile of nanopapillae on <i>Loxosceles</i> silk	30

Abstract

The spider *Loxosceles laeta* uses a choreography of its spinnerets to form its unique flat-ribbon silk into a series of loops. The series of loops is a one-dimensional thin-film mechanical metamaterial that undergoes strain-cycling by way of toughness increasing sacrificial bonds. The *Loxosceles* loop junctions are formed at $\bar{\theta}_C = 157.44^\circ \pm 5.40^\circ$ which is critically above the transition between the less tough peeling mode and the tougher lap shear joint delamination mode. The geometry of the loop junctions can be applied to thin-film materials at all length scales to increase toughness, allowing engineers to tune the toughness of this one-dimensional metamaterial.

Chapter 1

Introduction

Mechanical metamaterials are an enhanced class of materials that use unique structures to exhibit material properties which are superior to ordinary materials. Ultra-light, ultra-stiff metamaterials for example have reduced densities, but through a network of internal structures at different length-scales, are able to achieve their ultra-stiffness [1]. Taking a “bottom-up” engineering approach to mechanical metamaterials, with the fundamental internal structures at the micro- and nano- length-scales, allows for diverse bulk-material geometries [2]. Natural cell-based bio-materials such as cork and honeycomb have been the source of inspiration for designing such metamaterials [1]. Engineering ordinary materials to have a meta-structure can change or amplify the material properties.

Silk has proven to be an exceptional ordinary material [3], and has been used in both electromagnetic, and mechanical meta-materials [4], [5]. Spider webs are an example of a mechanical metamaterial; composed solely of silk threads, but when arranged in a web gives rise to the web’s ability to catch prey [6]. The web’s fundamental internal structures are the anchorages between dragline silk and the substrate, and the adhesion between fibers. The anchorages are optimized for the load and energetic capacity of the dragline silk [7], and silk-on-silk adhesive contacts improve the strength (i.e. load capacity) and toughness (i.e. energy capacity) of the web [8].

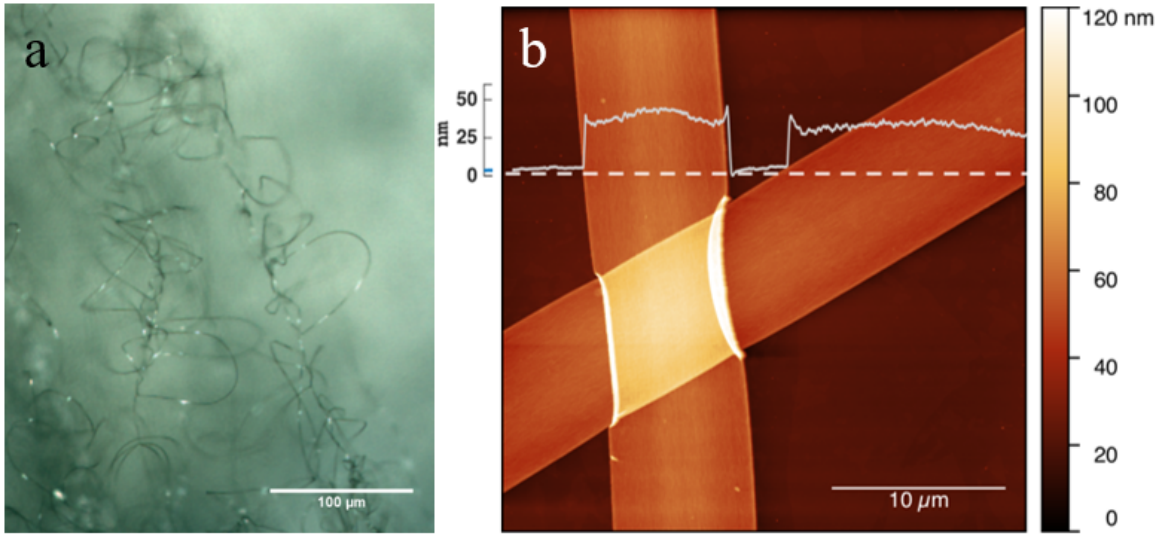


Figure 1.1: a) Optical microscopy (OM) image of series of *Loxosceles* loops at 5x magnification. This sample was collected directly from the spider's habitat. b) Atomic force microscopy (AFM) image of *Loxosceles* silk flat ribbon morphology: 60 nm by 7 μm. Shades of orange indicate height of the sample.

Large orb webs, however, are not the only meta-structure in which the silk can be arranged to achieve enhanced properties.

The main dragline silk of the spider *Loxosceles laeta* naturally forms a one-dimensional mechanical meta-structure. Unlike other spider silk, *Loxosceles* has a flat, ribbon-like morphology [9] that can be modeled as an elastic thin-film as seen in *Figure 1.1(b)*. The silk is spun using a choreography of spinnerets such that two regions of the same fiber are in adhesive contact to form loops at about 200 loops/cm as shown in *Figure 1.1(a)*, *Figure 1.2*, and *Figure 2.3*. The series of loops is the micro-structure of the metamaterial which increases the toughness of the silk by 30% [5]. This paper uses the *Loxosceles* loops as inspiration to investigate the viability of the loop system as a tunable one-dimensional metamaterial for other thin-films.

This one-dimensional metamaterial is able to increase toughness because hidden length from within a loop is exposed when the sacrificial bonds of the loop junctions fail [5]. Sacrificial bonds have been widely studied at the molecular level with polymer

chains which provides the molecular basis for tough bio-materials [10]–[12]. Two key differences between a polymer chain and *Loxosceles* silk with sacrificial bonds are 1) the source of pre-bond-failure stress and 2) the sacrificial bonds themselves. In a molecular system, the pre-bond-failure stress is due to entropic forces of elongating the molecule into a state with fewer microstates [10], while in the silk, the whole strand is strained [5]. The sacrificial bonds in molecular systems vary in strength from covalent bonds to weaker intermolecular interactions [10], [11], while the silk relies solely on the adhesion of the contact area, likely incorporating only intermolecular forces such as van der Waals interactions. Despite the differences in the mechanism, the result of increasing the toughness of both systems is the same. The fundamental principle is load-cycling which entails loading the material until a sacrificial bond fails, which exposes new length to relax the system until it is loaded again [5], [10]–[12]. The strain-cycling characteristics of the *Loxosceles* loops were explored by *Koebley* [5], but it is the thin-film mechanics of the sacrificial bonds which are described in this paper.

The adhesion of elastic thin-films is characterized by the work required to expose a unit area of the interface of the two surfaces [13]. Two mechanical methods to characterize the adhesion of thin-films are 1) a peel test where a force is applied at an angle relative to the substrate over a distance of delamination of the film [13]–[17], and 2) a tangential shear or lap shear method where force is applied along the film plane until complete delamination of the film [13], [18]–[26]. For elastic thin-films undergoing the peel test, there is an elastic term to the force that causes film-deformation at the peel front, which is negligible in the thin-film limit [14]–[16]. This paper determines the contact angle dependence on the delamination mechanics that causes the transition from peeling to a lap shear joint [17]. It is qualitatively observed that the adhesive contact area of the loops fails in these two independent

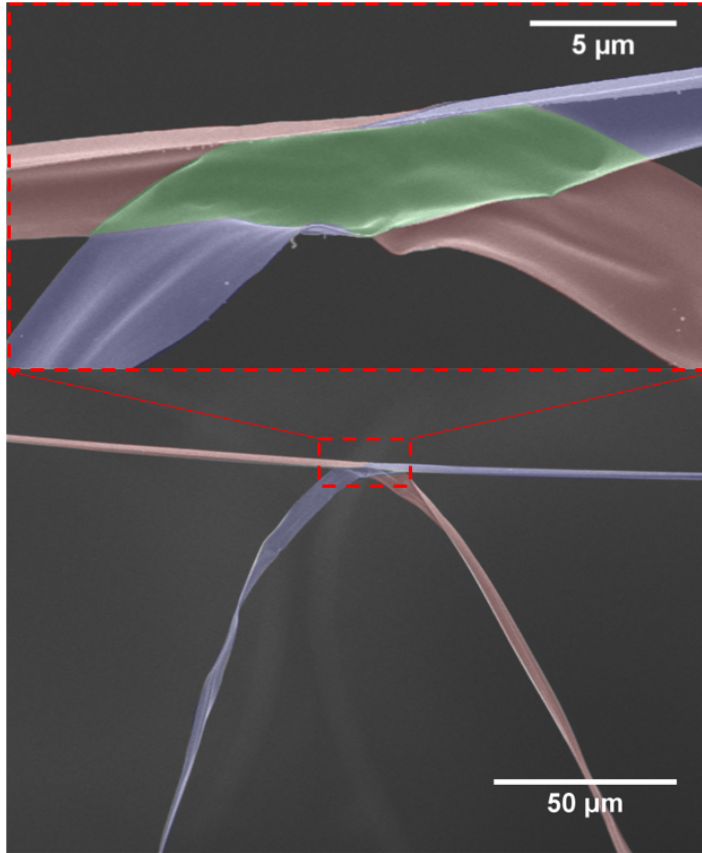


Figure 1.2: Scanning electron microscope images of a single *Loxosceles* loop. The top image is a closer look at the same loop junction shown below. The green region is the contact area of the two surfaces. The blue and red region is a single silk strand, but colored differently to show that the two sides behave independently and tensile force is applied in opposite directions. The very top of the image is an example of a cusp that has formed because the contact angle is too large to allow the silk to peel apart.

modes.

The adhesive contact area of the loops are the sacrificial bonds in this one-dimensional thin-film mechanical metamaterial, and are the fundamental internal structures upon which the metamaterial functions. This paper introduces analysis for preferred geometries of the contact areas for tunable toughness increase at all length scales based on detailed thin-film mechanics of loop failure. We also investigate the effectiveness of the *Loxosceles* loop system as this type of metamaterial.

Chapter 2

Theory

This chapter details the mechanics of a one-dimensional thin-film mechanical metamaterial. The criteria that allow the metastructure to be possible are that the material must 1) be a thin-film, 2) have sacrificial bonds, and 3) allow load-cycling. The combination of these three characteristics will allow for an ordinary material to become this metamaterial. The toughness of a material is defined as the area under a stress-strain curve, or how much energy it is able to absorb before failure. The increase is due to the peaks created by loading the backbone material until the sacrificial bonds fail as seen in *Figure 2.7*, which is only possible under these criteria.



Figure 2.1: Scanning electron microscopy (SEM) image of *Loxosceles* silk folded onto itself demonstrating the high flexibility of the thin-film.

2.1 Thin-Films

The criteria that the material be thin is relative to the length-scale. Spider silk has a tensile strength comparable to high-strength steel [3], and this may lead to the

assumption that the silk fibers are as rigid as a steel beam. When observing the silk at a length-scale of micrometers, it is highly flexible as seen in *Figure 2.1*. Because the silk is only 60 *nm* thick, it can maintain its strength while also being highly flexible. The tensile strength of a material is normalized by its cross-sectional area, therefore, this observation can be generalized to most materials; high-strength steel will become flexible when flattened to a thin-film [14].

Thin-films have application in systems where the film is in adhesive contact with a substrate. When a thin-film is stressed at an angle relative to the substrate (*Figure 2.2*), an elastic term of bending the material arises at the peel front where the material crimps onto itself [14]–[17]. The thickness of the material is directly proportional to this elastic term ($1 - \nu^2$), and so a thin-film has a reduced or negligible elastic effect around ridges of flexion where the crimping occurs [15]. Only when the material is thin enough to allow the elastic term at the ridges of flexion to be negligible will the thin-film criteria be satisfied for the metamaterial [14]. When this condition is not satisfied, the material is less likely to be able to form an adhesive contact in such a way to maximize surface area. The surface area is critical to the success of the sacrificial bonds of the metamaterial. The details of the surface area will be discussed later.

Kendall 1975 showed that for a rectangular geometry ($A = b \cdot \Delta c$) thin-film as shown in *Figure 2.2*, where the force is parallel to the delaminated film, the peel strength proportional to the peeling angle relative to the substrate [17]. The relationship between peel strength, F , and angle relative to the substrate, θ can be expressed as:

$$\left(\frac{F}{b}\right)^2 \frac{1}{2dE} + \frac{F}{b}(1 - \cos\theta) - R = 0. \quad (2.1)$$

In the above equation, d is the thin-film thickness, E is the elastic modulus of

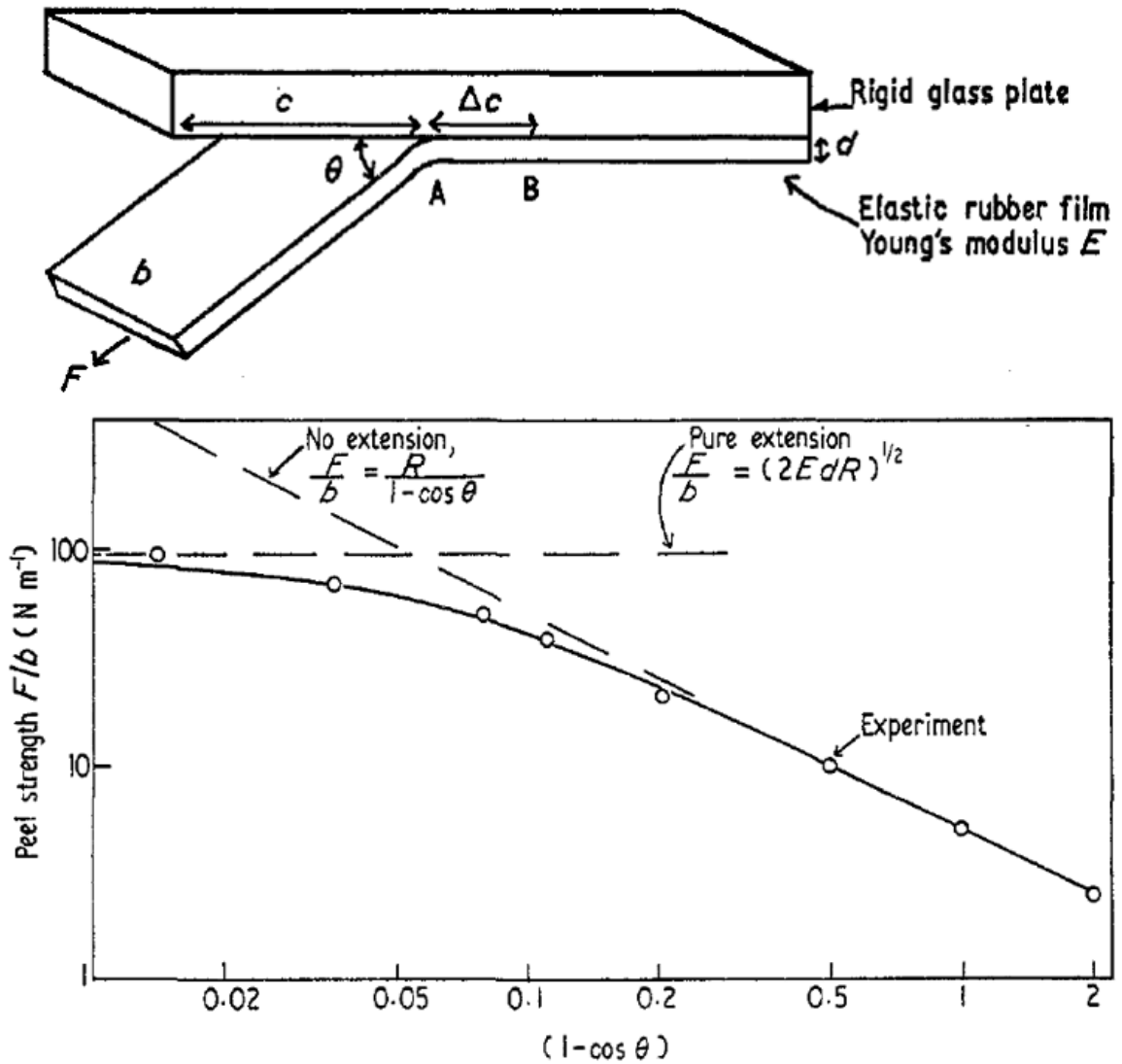


Figure 2.2: This is the model that *Kendall 1975* used for describing the peeling mechanics of a thin-film from a rigid substrate. The geometry is a square geometry where the area removed is the distance removed times the constant width of the film, $A = b \cdot \Delta c$. The plot shows *Equation 2.1*, peel strength as a function of the pulling angle. Adopted from *Kendall 1975* [17]

the thin-film, b is the width of the thin-film, and R is the surface energy, more commonly expressed as γ . *Figure 2.2* shows that the first term dominates at $\theta \approx 0^\circ$, and the second term dominates at $\theta \approx 90^\circ$. The first term is referred to as the pure extension term, where the applied force goes predominately to shear force at the adhesive interface and stretching the free section of the thin-film and behaves like a lap shear joint system. The second term is referred to as the no extension term where the system is strictly peeling, and there is little to no shear at the interface or stretching.

2.2 Sacrificial Bonds

Sacrificial bonds are simply bonds that break before the main structure of the material [27]. In this metamaterial system, the sacrificial bonds are the loop contact area adhesive bonds. With *Loxosceles* silk, the adhesive bonds are solely intermolecular, likely van der Waals [28], however, for a general system, the type of bond can range in strength from covalent to intermolecular and be any form of adhesion (mechanical, chemical, etc.) [10]. Despite this range of possible sacrificial bond types, they all must fail before the backbone of the metamaterial. This thesis investigates the geometry of the sacrificial bonds in the thin-film metamaterial. The loops of the metamaterials are formed at an angle which is defined as the obtuse angle of the rhombus formed when the contact area of the two surfaces meet to form the loop as shown in *Figure 2.3(a)*. The two modes of bond failure, as a function of loop angle, are peeling and shearing at an adhesive interface.

2.2.1 Peeling Delamination Mode

Under peeling regimes, the peeling front moves across the rhomboid contact area from one obtuse angle to the other obtuse angle as seen in *Figure 2.3(a)*. When comparing

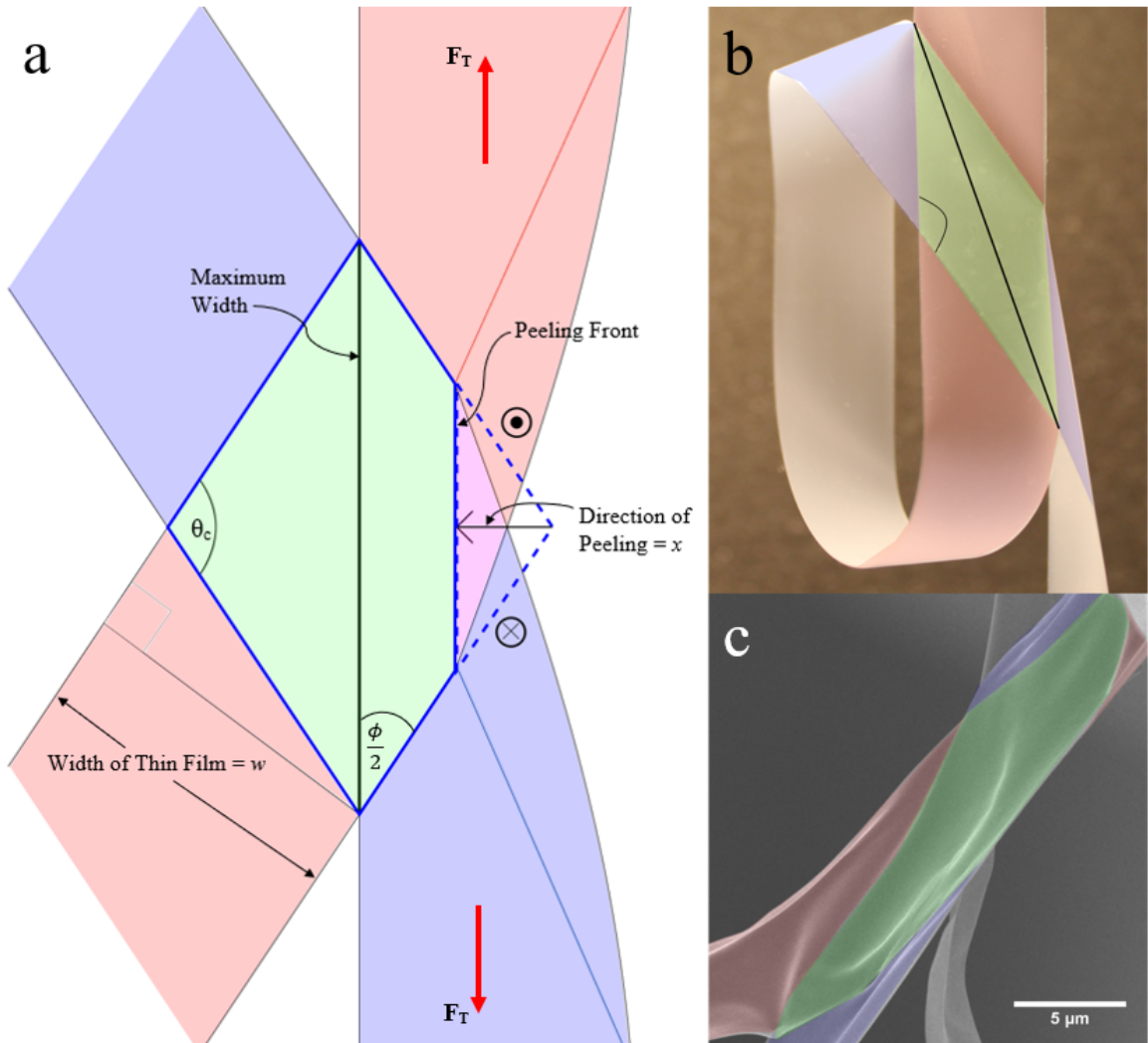


Figure 2.3: a) The peeling geometry of an angle less than the critical angle. The green region is where the two layers are in adhesive contact: the contact area. The red region is the top layer of the contact area. It originates where the loop is pinned above, and continues through the loop. The blue region is the bottom layer of the contact area and it originates from the loop and ends where the masses are hung to measure the force. The magenta region is delaminated film, but is overlapping in the z -direction. The two circles indicate the direction in the z -direction that the respective planes are oriented, dot: $+z$, and cross: $-z$. The red arrows labeled F_T indicate the direction of the tensile force applied to the loop. b) preliminary tensile test using tape as described in *Chapter 3.2* with correlated false colors to the contact area geometry in (a). c) Scanning electron microscopy (SEM) image of a *Loxosceles* silk loop junction with correlated false colors to the contact area geometry in (a). This is a similar image to *Figure 1.2*.

this geometry to the *Kendall 1975* model [17], the peeling direction is simply the distance delaminated ($\Delta c \rightarrow x$) times the length of the peeling front, which would be constant for the square geometry, but due to the rhomboid geometry, the peel front is not constant and a new geometry must be derived. The two surfaces are being peeled perpendicularly from the contact area, A . This means that, according to the *Kendall 1975* model, the peeling angle will be $\theta = 90^\circ$, which means the delamination is fully in the no extension mode, all peeling. According to thermodynamics, there is an energy penalty, U , for exposing new surface area as shown in *Equation 2.2*. From this we know that the surface energy, γ , is proportional to the new surface area being exposed [17].

$$F = -\frac{dU}{dx} \rightarrow \gamma = \frac{U}{A(x)} \therefore F(x) = -\gamma \frac{d}{dx} A(x) \quad (2.2)$$

The maximum force, F_{max} , required to expose more surface area occurs at the maximum width, x_{max} , of the contact area which is perpendicular to the x direction and is half way across the total contact area in the x direction. Therefore, the loop continues to complete failure once F_{max} is reached. The geometry of the newly exposed area as a function of the peeling direction x is:

$$A(x) = x^2 \cdot \cot \left(\frac{180^\circ - \theta_{contact}}{2} \equiv \frac{\phi}{2} \right) \in \left[0 \leq x \leq x_{max} = w \cdot \csc \phi \cdot \sin \frac{\phi}{2} \right] \quad (2.3)$$

$$F(x) = 2\gamma x \cot \left(\frac{\phi}{2} \right) \rightarrow F_{max} = 2\gamma w \cdot \csc \phi \cdot \cos \left(\frac{\phi}{2} \right) \quad (2.4)$$

Figure 2.4 shows graphical representations of the above equations for the tape used in *Chapter 3*. It can be seen that there is a definite F_{max} for a particular θ_c . For each trial, F_{max} and ϕ are constants, which will allow us to determine the surface energy per unit area (γ) of the thin film while in peeling mode delamination. Since $\gamma = \gamma(\dot{x})$, we will experimentally keep $\dot{x} = 50 \mu m/s$ constant for each rheometry trial [17]. \dot{x} was difficult to control for the preliminary tensile tests, so the experiments were

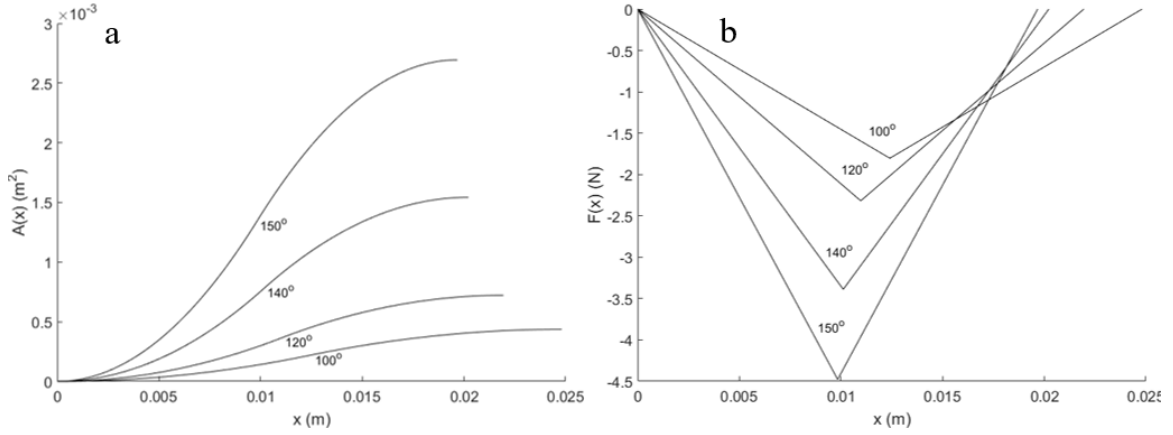


Figure 2.4: a) shows the contact area as a function of peel direction x according to *Equation 2.3*. b) is the peel force as a function of the peel direction x according to *Equation 2.4*. Both graphs include plots at four contact angles within domain of interest.

conducted over several minutes, to ensure slow delamination to reduce the impact of $\gamma(\dot{x})$.

2.2.2 Lap Shear Joint Delamination Mode

Lap-joints are composite structural components that bind two rigid structural elements together. However, as discussed above, thin-films by nature are flexible, not rigid. This problem is solved due to the geometric infeasibility of the peeling mode with shear forces, so the system behaves like a lap shear joint [17]. Peeling is possible due to the perpendicular orientation of delaminated film with respect to the contact area, however at larger contact angles, a cusp forms where peeling would originate, inhibiting peeling and creating conditions similar to shearing of a lap joint. This cusp is visible in *Figure 1.2*. The image is a loop junction at 155° contact angle under tension. There is no peeling possible because the two surfaces are joined at too great of an angle; forming the cusp, the top edge of the silk is loaded without the junction peeling apart.

Despite the change in geometry, the contact area is still defined by *Equation 2.3*

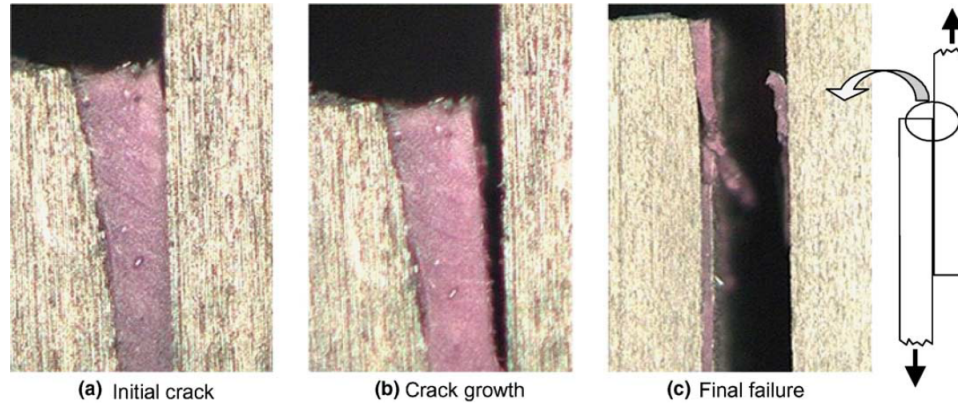


Figure 2.5: Single lap-joint failure using a secondary paste adhesive. Demonstrates the failure geometry of a lap shear joint that would be similar to loop junction failure at contact angles greater than the critical angle. The backing of the thin-film peels away from the substrate slowly until sudden and complete failure. Adopted from *Kim 2006* [18].

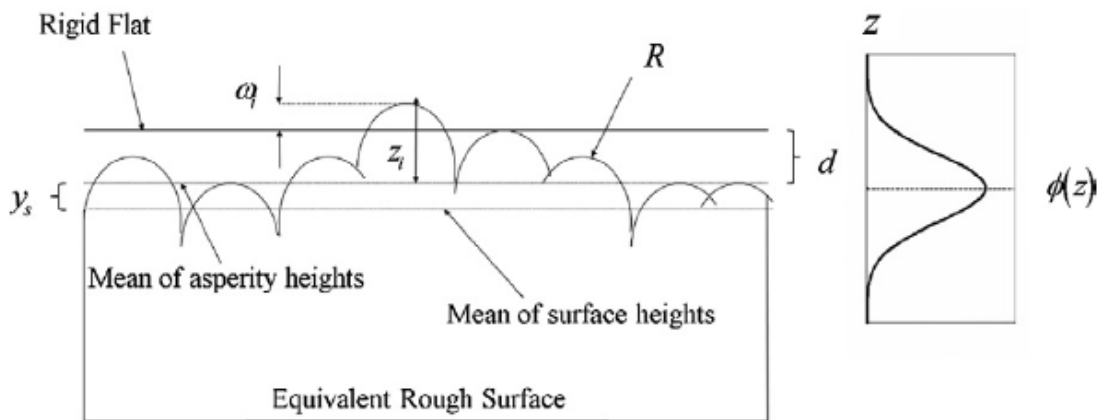


Figure 2.6: This model of two contacting rough surfaces is the basis for *Equations 2.5, 2.7, and 2.8*. $\phi(z)$ is a Gaussian distribution of the height of the asperities. The shape of the asperities in this model are approximated to be hemispheres all having constant radii R . Adopted from *Eriten 2011* [25].

and is still the sacrificial bond, however, instead of the adhesive surface energy, it is frictional surface asperities that are the mechanism behind the sacrificial bond. The sacrificial bond still must fail before the material fiber, therefore there must be stable delamination originating from both ends of the contact area that extends between the adhesive and the adherend until complete failure [18]. The contact area will fail leaving the backbone material undamaged as seen in *Figure 2.5*. With the lap shear joint mode, roughness plays an integral role when modeling the force required to open a loop [18]–[26]. *Kim 2006* used the grit of sandpaper on a rigid substrate as the reference of surface roughness and concluded that finer grains of sandpaper correlates to less roughness and an increase in joint strength [18]. When looking at *Loxosceles* silk, however, roughness is on the *nm* scale while sandpaper has *μm* scale roughness, we can conclude that the smaller roughness features or asperities, will result in an increase in joint strength. The difference in the length-scale and effect of surface asperities on joint strength has been widely studied for rigid on rigid interfaces [18], [19] elastic on rigid [20]–[23], and general cases [24]–[26].

A major theme of this work is that characterizing the roughness is critical to developing a complete model of the system. *Figure 2.6* shows the model which is underlying basis for two rough surfaces in contact. Several assumptions made in this model are 1) the materials are isotropic, 2) asperities are spherical and have constant radii at their peaks, 3) asperities are far apart and are non-interacting, and 4) there is no bulk deformation [23]. It has also been shown that a system of two rough surfaces can be modeled by an equivalently rough surface in contact with a smooth plane [29]. Using the work of *Kogut 2004*, who continued work from the *GW* theory [20], the asperities follow the following distribution [24]:

$$\phi(z) = \frac{1}{\sigma_s \sqrt{2\pi}} \exp\left(-\frac{z^2}{\sigma_s^2}\right). \quad (2.5)$$

z is the distance from the peak of an asperity to the average height of all asperities, σ_s is the standard deviation of asperity heights. $\phi(z)$ can be applied to *GW* theory to determine the real contact area, or actual area physically in contact [20]:

$$A = \pi\eta A_n R \int_d^\infty (z - d)\phi(z)dz \quad (2.6)$$

where A_n is the nominal contact area which is the macroscopic area in contact which is determined using *Equation 2.3*. This equation supports the idea that flexible thin-films are able to maximize this real contact area better than rigid bulk materials and improve the adhesion. d is the separation of the two surfaces. This distribution is used to calculate the maximum force at failure of the lap shear joint using [24]:

$$F_{max} = \eta A_n \int_d^{d+6\omega_c} \bar{F}_{max}(z)\phi(z)dz. \quad (2.7)$$

η is the area density of asperities. $\omega_c = (\frac{\pi KH}{2E})^2 R$ is the critical interference that shifts the system from elastic to plastic deformation. R is the radius of curvature of the asperities, K and H are the hardness of the materials $H = 0.454 + 0.41\nu$, and E is the Hertz elastic modulus, $\frac{1}{E} = \frac{1-\nu_1^2}{E_1} + \frac{1-\nu_2^2}{E_2}$. In the case of this system, where the materials are in cohesive contact: $H = K$ and $E = \frac{E}{2(1-\nu^2)}$, thus $\omega_c = (\frac{\pi H^2(1-\nu^2)}{E})^2 R$. In *Equation 2.7*, \bar{F}_{max} is static frictional force of each individual asperity which is calculated at the level of the individual asperity. For this model, a fully elastic regime was used, so \bar{F}_{max} can be expressed as [24]:

$$\bar{F}_{max}(z) = \bar{P}_c \cdot a_i \left(\frac{z - d}{\omega_c} \right)^{b_i}. \quad (2.8)$$

In the above equation, $\bar{P}_c = (2/3)KH\pi\omega_c R$ is the critical contact load at yield, and as discussed above, since the material is in cohesive contact, $K = H$. a_i and b_i are constants and vary depending on the model of deformation. Since the silk will stay in a fully elastic regime, $a_i = 0.52$ and $b_i = 0.982$ [24]. The combination of

Equations 2.5, 2.6, 2.7, and 2.8 give a complete analytical solution to the lap shear joint delamination mode.

The modulus, E of *Loxosceles* silk has been determined to be $21 \pm 6 \text{ GPa}$ [9] and the axial Poisson ratio can be approximated based off other spider silk fibers, $\nu = 0.67$ [30]. These parameters of the surface roughness for *Loxosceles* silk and the tape used experimentally are determined experimentally and will be discussed in *Chapter 3*.

2.3 Strain-Cycling

The combination of the preceding two criteria (thin-film and sacrificial bonds) over a series of loops will naturally give rise to a cyclic process of toughness increasing peaks in a stress-strain curve. The length-scale determines the mechanisms behind this phenomenon as described in the introduction. Molecular systems have pre-bond-failure stress due to entropic forces trying to restore the molecule to a state with higher entropy. The entropic restoring force increases until a sacrificial bond fails where new length is exposed, allowing entropic forces to dominate and relax the molecule into a more random state now with more length, until the process repeats [10]–[12]. At the molecular level, this is not strain-cycling because the backbone of the system is not strained, the molecule is elongated.

At length-scales greater than the molecular level, we observe the strain-cycling where the backbone of the metamaterial is stretched until a sacrificial bond fails and new length is exposed which relaxes the fiber and then allows the material to be restrained as seen in *Figure 2.7* [5]. A key factor to consider is whether the backbone material is elastically, or plastically strained. Experiment indicates that *Loxosceles* silk is elastically strained which allows for uniform strain-cycling through the process [5]. If inelastic strain occurs, then each new peak would be reduced due to the plastic deformation caused by the initial inelastic strain. An ideal sample of the proposed

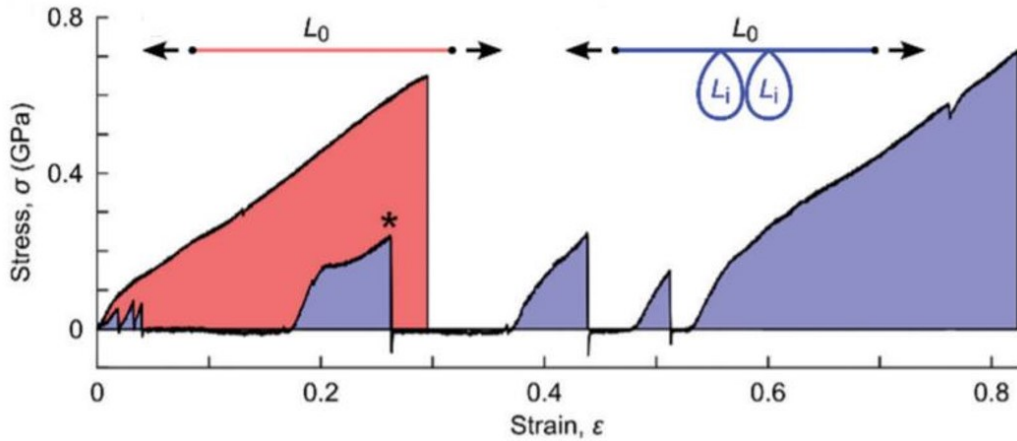


Figure 2.7: Stress-Strain curve of looped (purple) and unlooped (red) *Loxosceles* silk. A smaller purple peak indicates a loop opening and allowing the silk to be relaxed and strained further without stress until the slack from the exposed length from the opened loop is removed and the silk is loaded again. The total area or toughness under the looped curve is greater than that of the unlooped curve. Adopted from *Koebly 2017* [5].

metamaterial would be exclusively elastically strained with no plastic deformation for maximum toughness increase.

As demonstrated in *Figure 2.7*, we see that due to the addition of the loop structure, there is an increase in the area under the curve. The area, or integral of the stress-strain data gives the toughness of the material, or the amount of energy the material is able to absorb. The *Loxosceles* loops have been experimentally demonstrated to have a 30% increase in toughness due to the loops [5].

The uniform shape of loop opening events on the stress-strain curve indicates that the loops are able to fail such that the backbone is undamaged. This gives support to sacrificial bonds as integral structures to the metamaterial because the backbone material must still be in sufficient condition to allow for final loading of the unstructured material. In molecular systems, the sacrificial bonds are able to reform when stress is removed [10]–[12]. This property would be ideal, however unrealistic at larger length-scales due to the precise geometry of the loop junctions.

Chapter 3

Experimental Technique

3.1 Imaging

Imaging is critical to this project because it allows us to visualize and intuit the mechanics of the system. The first step in imaging is proper sample collection and preparation. The *Loxosceles* silk seen in *Figure 1.1* was collected directly from the housing capsule of the spider. The silk was removed from the capsule by using forceps and a hot wire to cut the section of loops away. The silk was then mounted on a scanning electron microscope (SEM) sample holder with two rolls of carbon tape to elevate the loops to ensure they remain undamaged. The sample was then placed on the Olympus iX71 inverted optical microscope (OM) using the 5x (*Figure 1.1*) and 20x (*Figure 3.2(a)* and *3.2(b)*) objectives.

To achieve high resolution images of loop junctions themselves, SEM was employed. The SEM used was the Hitachi S-4700 FE-SEM (field emission-SEM) from William and Mary's Applied Science Department as seen in *Figure 3.1(b)*. The samples were first sputter coated for 2 minutes using a gold-palladium target in a high-vacuum argon environment to allow for the sample to be conductive as seen in *Figure 3.1(a)*. The samples were then re-imaged using the OM to check for damage to the silk due to the sputter coating process. As shown in *Figure 3.2*, there is little evidence

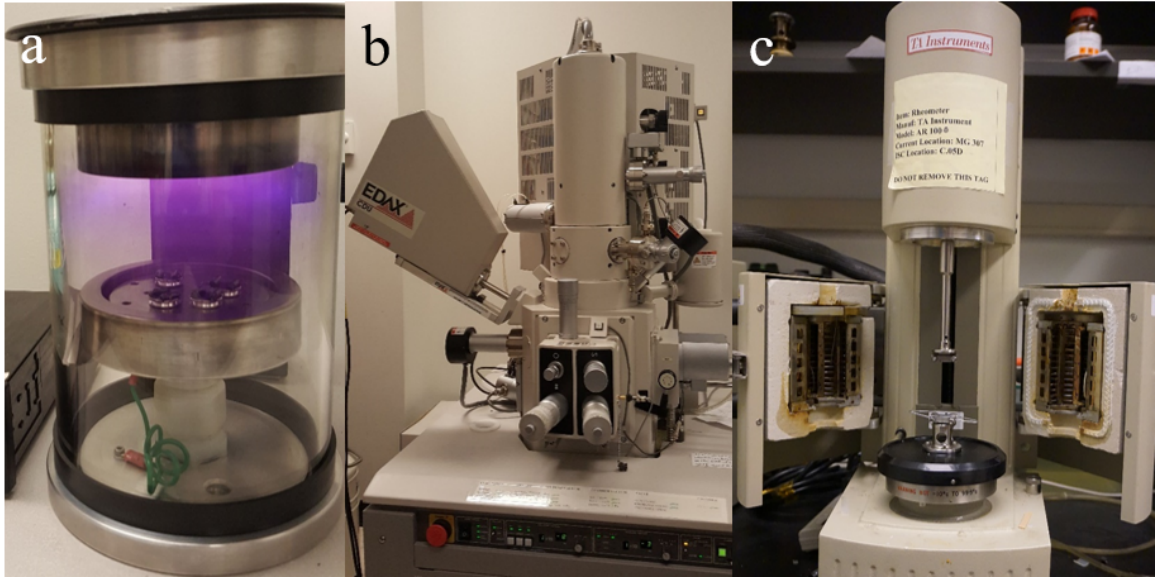


Figure 3.1: a) Sputter coater coating four silk samples. The purple haze is the Argon ionizing from the Au-Pd plasma. b) Hitachi S-4700 FE-SEM used for high-resolution imaging. c) TA Instruments AR 100 Rheometer used in high-precision tensile test

of severe damage to the loops. The samples were imaged under a 2 – 5 kV electron beam so that there would be less damage to the only slightly conductive and fragile samples. We were able to get magnifications up to 100 kx using the lower energy electron beam.

All images were processed using the open source software Fiji/ImageJ. This software allows for detailed measurements of images and adds scale bars onto images. This software particularly aided in the measurement of the contact angle of the SEM images. This helped develop statistics on the *Loxosceles* loop junctions. All data analysis was done using MATLAB (Mathworks, Inc.). It is a powerful tool for data analysis and plotting which can be seen in *Figures 2.4, 4.1, 4.2, 4.4, 4.6*.

To obtain topological data, atomic force microscopy (AFM) techniques were used. AFM uses an atomically sharp cantilever to scan over the surface of a sample. The height data is plotted using a variational color scheme using the open source software for AFM data analysis: Gwyddion as seen in *Figure 1.1(b)* and *Figure 4.5*. AFM

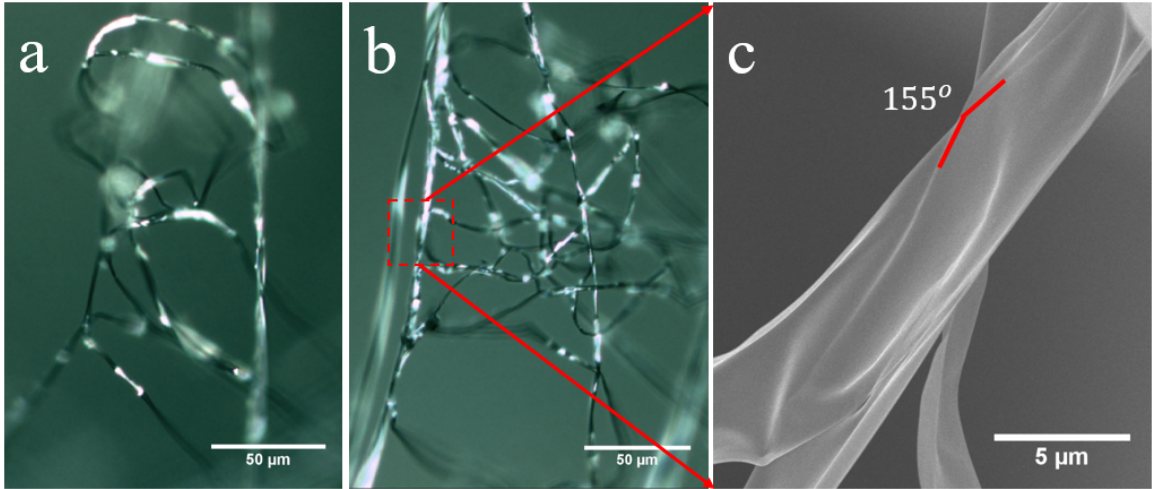


Figure 3.2: a) OM image of *Loxosceles* silk at 20x magnification before sputter coating process. b) OM image of *Loxosceles* silk at 20x magnification after sputter coating. Little damage was done to loops or the loop junctions by the sputter coating. c) SEM image of *Loxosceles* silk loop junction at 5kx highlighting that the contact angle is 155° .

is sensitive to height changes on the atomic level, so when scanning the surface of *Loxosceles* silk, it is able to capture small details at a high resolution. I am not trained to use the AFM, so I used existing data collected by Ph.D. candidate Qijue Wang for the *Loxosceles* data, and Ph.D. candidate Dinidu Perera scanned the tape used. This data can be used to calculate roughness parameters useful in developing the mechanics for the lap shear joint in *Equation 2.5* and *Equation 2.7*.

3.2 Preliminary Tensile Test

This experiment tested the effect of contact angle on the strength of a thin-film loop. The thin-film used was 3M™Scotch®Transparent Film Tape 600. According to the manufacturer, the tape is $58 \mu\text{m}$ thick and 19 mm wide. The manufacturer also reports a tensile strength of 49 N/cm , Poisson ratio, $\nu = 0.499$, and elongation at break to be 45% [31]. This tape satisfies the thin film criteria with a thickness to width ratio of about 1 : 300 which is two times less than to the *Loxosceles* silk aspect

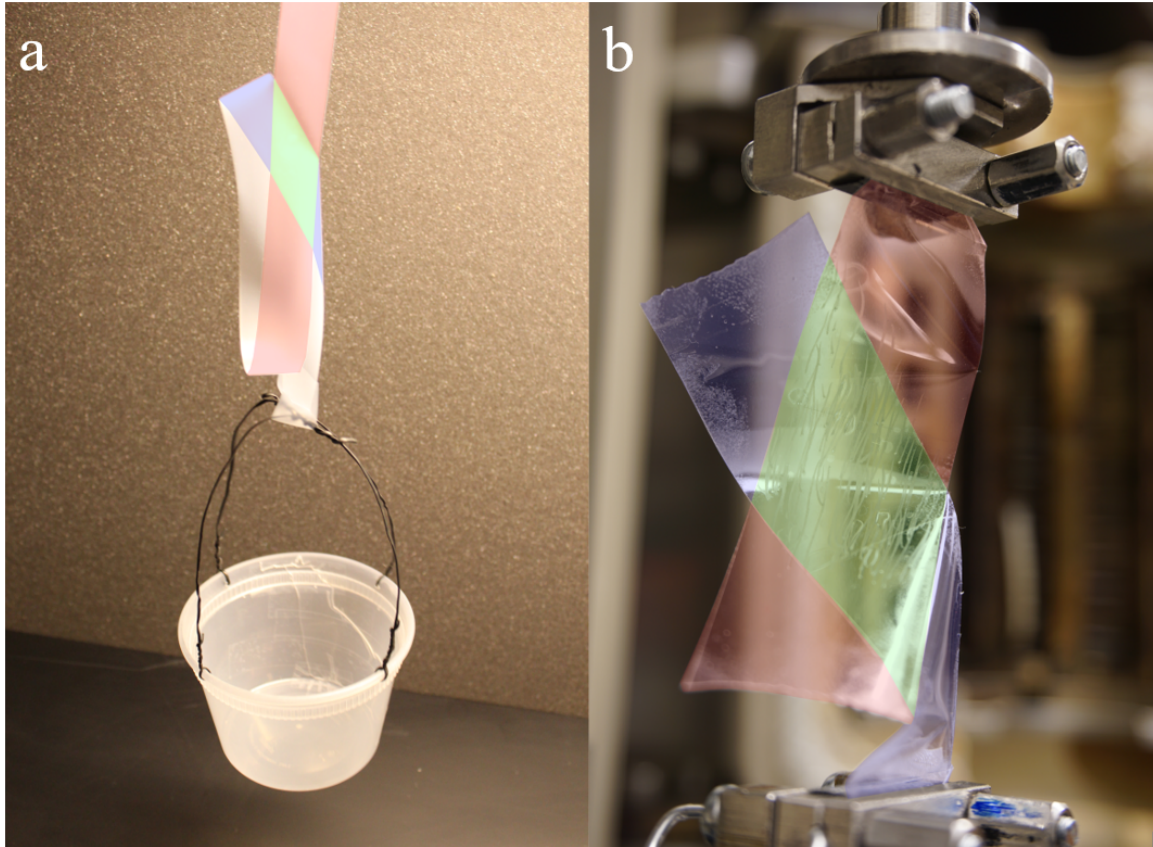


Figure 3.3: Experimental setup for preliminary and high precision tensile tests. a) shows the set up for the preliminary tensile test. Mass was added to the basket until the loop junction failed. The tape was adhered above to a lab table shelf. b) shows the set up for the high precision tensile test and includes the heads of the rheometer shown in *Figure 3.1 (c)* which holds the sample. For this sample, $\theta_C = 130^\circ$. Two independent sections of tape were adhered to form the contact area. A complete loop is not necessary to conduct experiments on the mechanics of the loop junction.

ratio which has range 1 : 100 – 1 : 150 [9]. The extensibility of the tape, however, is two times that of the *Loxosceles* at 27.4% [9].

For the experiment as shown in *Figure 3.3(a)*, a section of tape (≈ 30 cm) was shaped into a loop such that the adhered contact area had a contact angle as seen in *Figure 2.3(b)*. The looped tape was then secured above allowing the loop to dangle down and a basket was attached to the loose end of the tape (*Figure 3.3(a)*). Mass was added slowly to the basket until the loop failed. The total mass, including the mass of the basket, was recorded and converted to the maximum force at loop failure: $F_{max} = m_{hanging} \cdot g$. The contact angle was varied per trial from $90^\circ \leq \theta_C \leq 160^\circ$. Angles below 90° were not viable because the acute angle would clearly peel and not behave in a one-dimensional manner. Angles above 160° were not included due to length restrictions on the distance from the shelf to the lab table. As the contact area increased, there was more material being strained at 45% extensibility which exceeded the range of the testing apparatus. The purpose of this tensile experiment was to test the effect of contact angle on the strength of a thin-film loop, and to determine the angle at which the system transitions from peeling mode to lap shear joint mode delamination.

3.3 High Precision Tensile Test

The preliminary tensile test was an efficient way to observe the general trend of the effect of contact angle on loop strength. Each trial yielded one measurement: F_{max} , but did not test the validity of the peeling mode model. In order to measure the entire peeling regime, a TA Instruments AR 100 Rheometer (*Figure 3.1(c)*) was used in a monotonic ramp pull test. A rheometer is a machine designed to measure torsional forces. The top head is mounted on an air bearing to allow for free rotation in order to measure material properties such as viscosity and shear modulus. Due to the air

bearing, the machine is sensitive to forces in the range of $\{1 \mu N, 50 N\}$. This is the sensitivity range ideal for the Scotch®tape which has a tensile strength of $49 N/cm$ [31], and the loops would expect to fail at about half of that. The high resolution force measurements will test the peeling model for loop failure.

A challenge that the rheometer poses is that the maximum range of the moving head is $8.7 cm$. The Scotch®tape has high extensibility at 45% elongation at break [31], which means that for an unlooped sample, the unstrained length cannot exceed $6 cm$. This constraint limits the range of testable angles with the rheometer, for example: $\theta_c = 150^\circ$ has a maximum width of $7.345 cm$ according to *Equation 2.3*, only leaving $1.36 cm$ for the sample to be pulled, which is not enough distance to pull the sample to failure. This sample could still be tested, but data can only be collected from a small range. To obtain a complete trial without any elongation, the maximum angle that would be testable in the rheometer to peel the sample to failure, ($displacement_{max} = maximumwidth + 2 \cdot x_{max} \leq 8.7 cm$), would be $\theta_c = 147.2^\circ$, which means that only peeling regime contact angles can be tested. This maximum angle can be extended to 151.6° , because once the sample has reached F_{max} along x , it should symmetrically continue its peel. Using the example in *Figure 3.3(b)*, where $\theta_C = 130^\circ$, the maximum width is $4.8 cm$. Therefore, we would expect to just barely be able to measure the complete area delamination.

Each test was conducted using the same 3M™Scotch®Transparent Film Tape 600 as the preliminary tensile tests. Each sample was secured in the the square geometry of the rheometer using a $120 cN \cdot m$ torque wrench to ensure all connections are even to prevent bending or slipping at the grips as shown in *Figure 3.3(b)*. The rheometer displaced $50 \mu m/s$ and took measurements every second. Ideally, there would be a more continuous series of data points, but there was a limit to how quickly the machine could record data.

Chapter 4

Results

As discussed in *Chapter 2.2* the two modes of delamination are peeling mode and lap shear joint mode. Under the peeling mode, the maximum force of loop failure, F_{max} , is directly proportional to the surface energy, γ , as shown in *Equation 2.4*. Using the data from the preliminary tensile test that observationally failed under the peeling regime, $y = F_{max}$ vs $x(\phi) = 2w \cdot \csc \phi \cdot \cos \frac{\phi}{2}$ was plotted so that the slope of the plot is γ . *Figure 4.1* shows this plot with a linear fit for $\gamma = 61 \pm 6.23 \text{ J/m}^2$. The y error bars are $+0.2 \text{ N}$ and -1 N because when adding mass to the stage there was a greater likelihood that more weight was added and the loop failed faster, resulting in the recorded F_{max} being higher than the actual. Therefore, there is more error below the recorded data point. The error for γ was reported using a 95% confidence interval. The linear fit had a reduced $\chi^2 = 0.1545$ with 22 degrees of freedom which shows the strength of the fit. The full linear fit gave: $y = 61x - 0.76$, which includes a vertical shift in the fit, $y(0) \neq 0$, not addressed in the mathematics. There is no physical interpretation of this mathematical occurrence and with more data, this could be investigated.

In *Figure 4.2*, the black data points with error bars are the data from the preliminary tensile test. The blue trend line shows a regression for the peeling mode and is $F_{max}(\theta_C, \gamma)$. The function uses the extrapolated γ from *Figure 4.1* according to

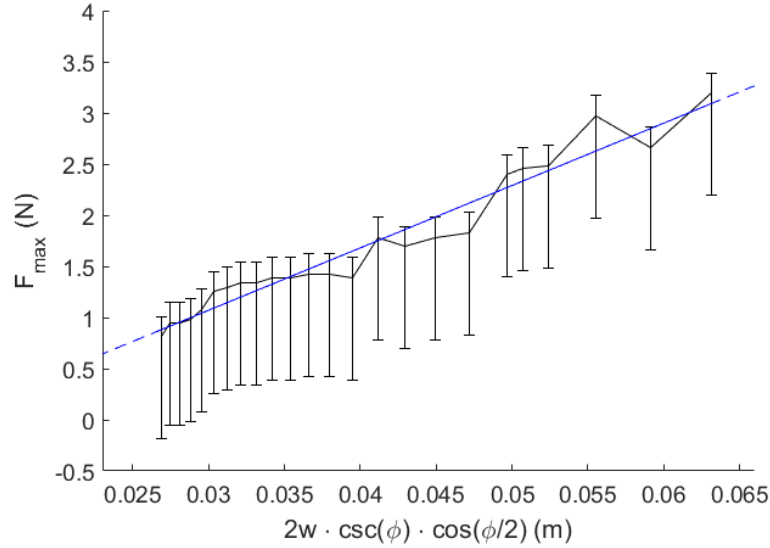


Figure 4.1: Peeling data from preliminary tensile test plotted with a linear fit to determine the surface energy of the tape system, $\gamma = 61 \pm 6.23 \text{ J/m}^2$. The geometry is such that F_{max} is linearly dependent on the contact angle expression on the x -axis which is determined by *Figure 2.4*.

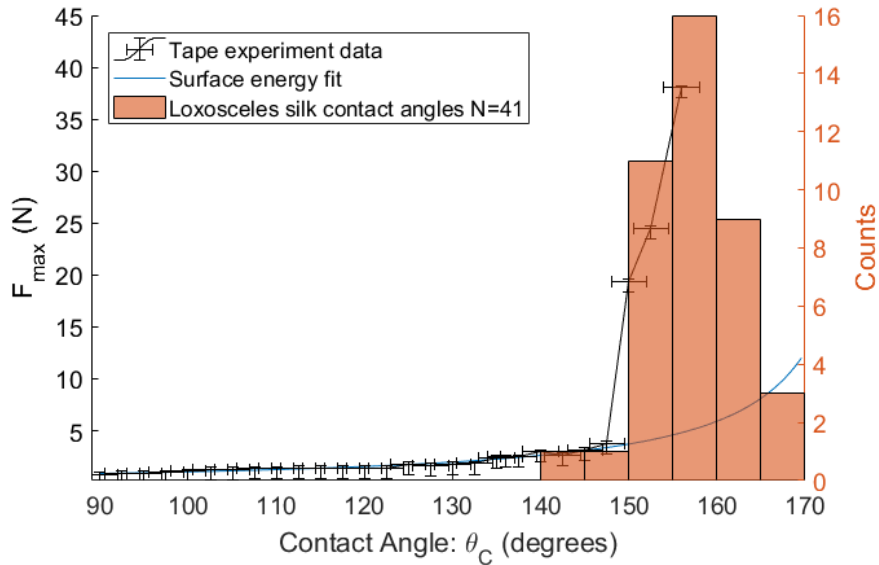


Figure 4.2: Plot combining data from the preliminary tensile test, peeling model, and imaging of *Loxosceles* loop junctions. The black data with error bars is experimental data directly from the preliminary tensile test as F_{max} vs. θ_C . The blue trendline is a fitted plot of the surface energy, extrapolated from *Figure 4.1* for peeling mode delamination, also using the left y -axis. The orange histogram uses the right y -axis and shows the data collected from measuring 41 *Loxosceles* loop contact angles.

Equation 2.4. At $\theta_C \geq 147.5^\circ$, the experimental data diverges significantly from the fitted trend line, which indicates that there is a sharp transition from peeling mode to lap shear joint mode, where F_{max} is no longer directly proportional to $A(\theta_C)$. The divergence from peeling mode to lap shear joint mode increases the required force to open a loop $10\times$. This transition is possible by a small increase in contact angle above 147.5° . Due to the resolution of the angles used in this experiment, we can only conclude that the critical angle at which the transition occurs is $145^\circ \leq \theta_C \leq 147.5^\circ$. The x error bars for the experimental data are $\pm 2^\circ$ because the tape was difficult to work with which led to the error in the angle measurement and loop formation.

Figure 4.2 also includes a histogram of contact angles from *Loxosceles* silk loop junctions. This data was collected from the SEM imaging discussed in *Chapter 3.1*. The *Loxosceles* data has an average angle of $\bar{\theta}_C = 157.44^\circ$ and a standard deviation of $\sigma_{\theta_C} = 5.40^\circ$. The SEM imaging has produced $N = 41$ loop junctions, which indicates the strength of the statistics.

Figure 4.3 is a representative trial from the high precision tensile tests. This particular trial had $\theta_C = 105^\circ$, so we should expect the system to be completely in peeling mode. First, there is the red, force vs. linear displacement curve that has a vertical shift in the data due to the the zero force point on the machine not being properly calibrated for this trial. As a result of this, the data points referred to will be corrected by repositioning the minimum force data point to be at zero force, a shift by $-0.54 N$. The first valley at about $-2.15 N$ and the second valley at $-1.15 N$. These values for the valleys are reported as negative due to the inversion of the rheometer used; pull/tensile tests report negative forces, and squeeze/compression tests report positive forces. According to *Equation 2.4*, $F_{max}(105^\circ) = 1.144 N$, which agrees with the magnitude of the second valley. This offers support to the validity of the peeling model proposed in *Chapter 2.2.1*. According to the theory however,

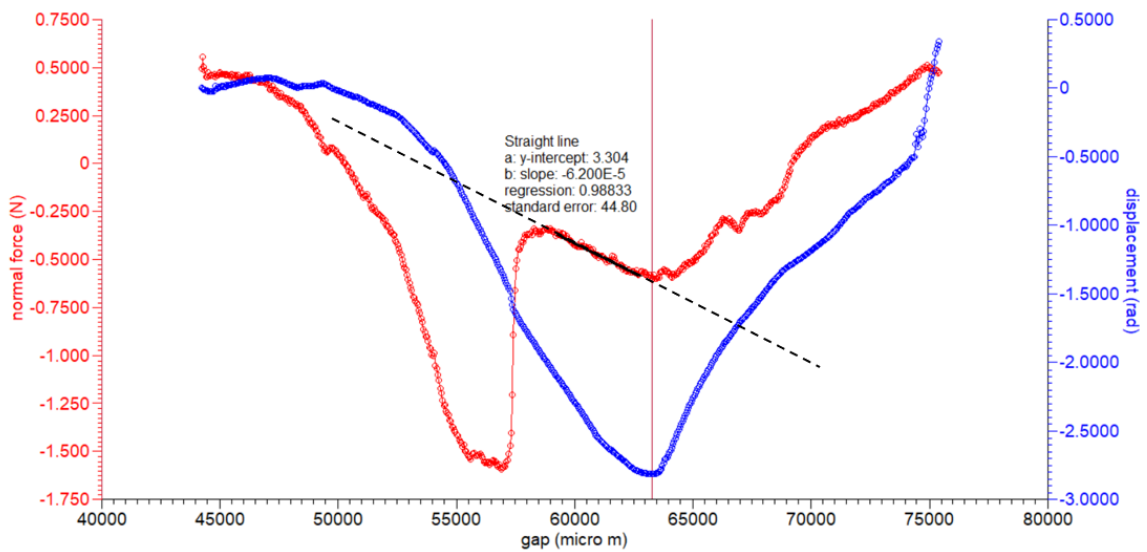


Figure 4.3: Representative trial of a high precision tensile test with $\theta_c = 105^\circ$ using the rheometer shown in *Figure 3.1(c)*. The red curve is normal force vs. linear displacement. There is a vertical shift in this data due to the zero force point not being properly set on the machine. The blue curve is angular displacement vs. linear displacement. The black line is a linear fit of the represented section of data with $m = -6.2 \times 10^{-5} N/\mu m$ and regression value of 0.988. The reference line indicates the correlation between the minimum of displacement and the theoretical maximum force.

the absolute maximum force should occur there, while the experimentally measured maximum force for this geometry was the first valley, almost two times greater than the expected F_{max} . This is due to an annealing process of the sample as the trial progressed where the system is able to adjust to find a lower energy state. Because the rheometer head is on the air bearing and is free to rotate so that over the course of the trial, the sample will rotate to find an orientation of least force. This rotational data is the blue angular displacement vs. linear displacement. It can be seen in *Figure 4.3* that the first valley corresponds to the sample having a cusp at the location where peeling should begin. This results in the sample being strained without much rotation through the first valley. The sample then releases the cusp, allowing the tape to relax in a lower stress state. After this one annealing phase, the sample then begins to peel to through the second valley, then symmetrically proceeds failure as expected by the theory. The valley that corresponds with the theoretical maximum was determined by the angular displacement data. The vertical reference line indicates the minimum of the angular displacement, which perfectly aligns with the second valley: the theoretical F_{max} .

The agreement of this trial with the theory is demonstrated by the black trend line on *Figure 4.3* which encompasses the period of the trial that followed the theoretical regime. The slope of the line is $m = -6.2 \times 10^{-5} \text{ N}/\mu\text{m} \rightarrow 62 \text{ J}/\text{m}^2$ and has a regression value of 0.988. This indicates that the surface energy calculated using the preliminary data ($\gamma = 61 \pm 6.23 \text{ J}/\text{m}^2$) agrees with the high precision data because it is within the 95% confidence interval. The regression value shows the strength of the linear fitting plot.

When directly comparing the preliminary tensile tests to the high precision tensile tests, only the F_{max} can be compared. *Figure 4.4* is an overlay of data sets from both experiments. The corrected blue data points are in strong agreement with the pre-

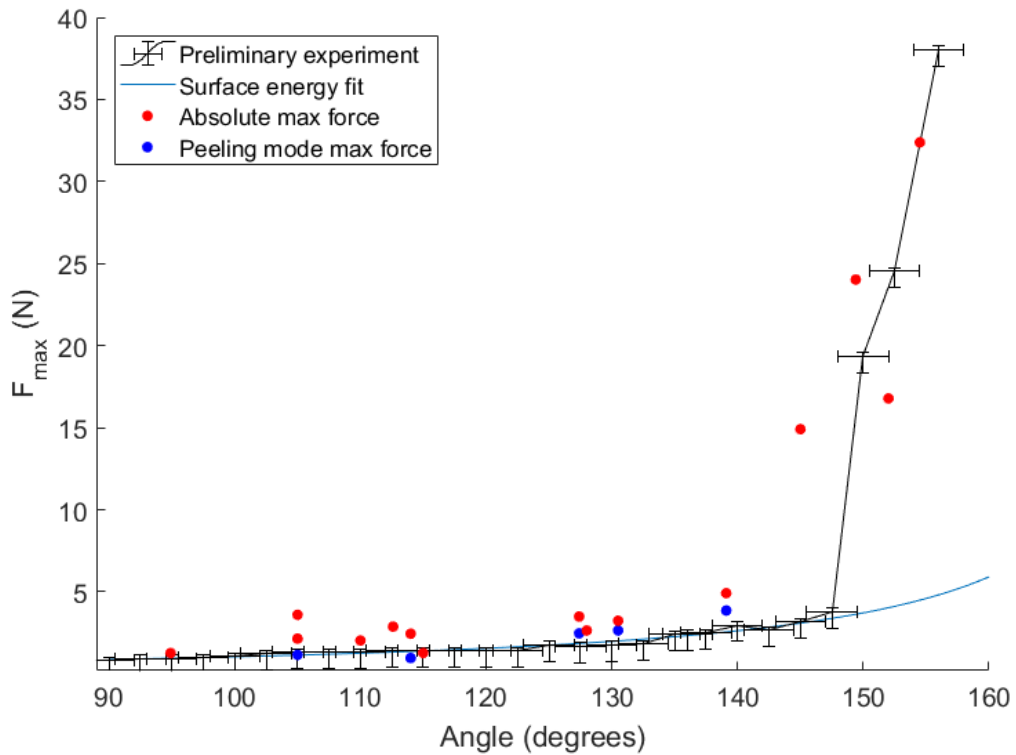


Figure 4.4: Black error bars and blue trendline is the same from *Figure 4.2* representing preliminary tensile test data and theoretical F_{max} . Red data points are the absolute maximum force measurements from the rheometer, while blue data points are adjusted, taking into account the annealing process. The difference in the two points is determined by the minimum of the angular displacement data aligning with the theoretical F_{max} .

liminary test and theory for peeling mode delamination. The main difference comes with the annealing process which allows the loop to support, in some cases, $4\times$ the theorized force. The red data points indicate the absolute maximum force determined by the rheometer. There are no instances where the annealing process causes F_{max} to be less than the theorized value. This difference in the annealing process vs. theory gives a plausible explanation for why the *Loxosceles* loops are sometimes formed at below the critical transition angle as shown in *Figure 4.2*. There is a possibility for smaller angles to still handle significantly larger loads if a cusp, shown in *Figure 1.2*, forms where the theory does not expect one. The preliminary tensile test did not see any deviation from the theory below the critical angle because the trials were conducted over a long enough time scale so that the annealing occurred before F_{max} measurement could be taken. These characteristics of the annealing process indicates that the real F_{max} force will on average be greater than the theoretical. This supports the idea that at large contact angles, where a cusp is guaranteed to form, the force required to open the loop will always be greater than the peeling mode theory and, therefore, need the lap shear joint mechanics of frictional forces acting on rough surfaces as described in *Chapter 2.2.2*.

Parameters required to determine an analytical solution for the lap shear mode include: area density of asperities, η , standard deviation of the roughness, σ_s , elastic modulus, E , and Poisson ratio, ν . For the tape used experimentally, $E = 49 \text{ N/cm}$ and $\nu = 0.499$ which are known from the manufacturer [31]. The roughness parameters required were determined experimentally by using AFM techniques as seen in *Figure 4.5(a)*. Using $N = 3$ samples, the root-mean-squared (RMS) roughness = 2.671 nm could be determined but since there are no punctuated asperities apparent on the tape surface, η , could not be determined.

AFM imaging was also done to examine the roughness parameters of the *Loxosceles*

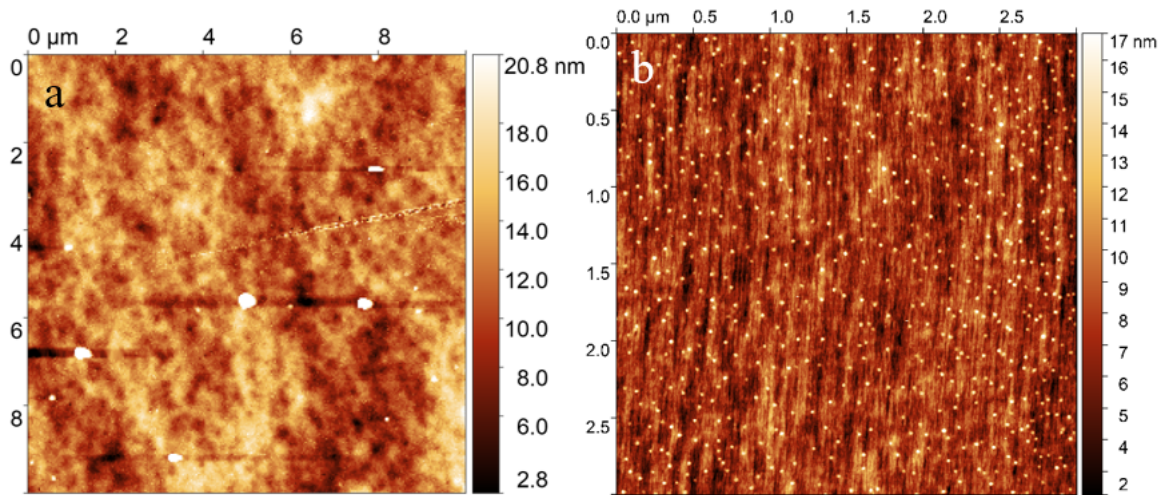


Figure 4.5: a) AFM scan of the surface of 3MTMScotch[®]Transparent Film Tape 600. The large elevated features are likely debris from sample preparation, and not regular asperities of the tape. b) AFM scan of the surface of *Loxosceles* silk. The raised yellow dots are called nano-papillae, they protrude $8.89 \pm 1.63 \text{ nm}$ from the surface of the silk [9]. The tape has larger roughness features but are that are not as punctuated as the nano-papillae.

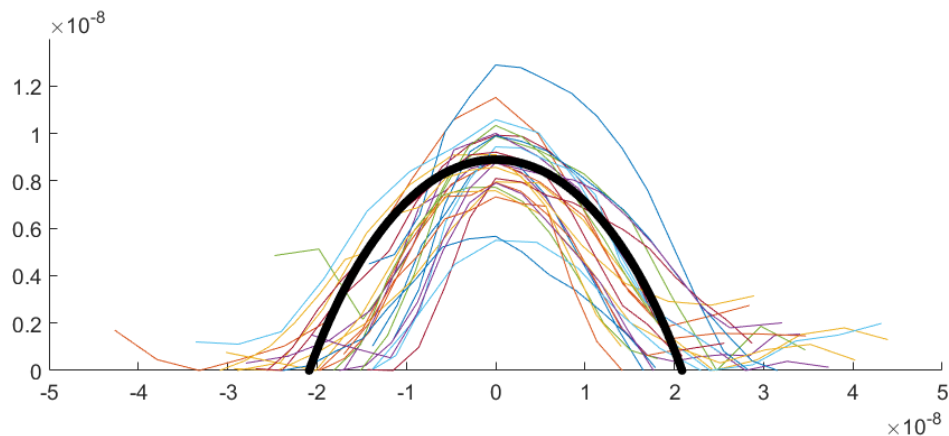


Figure 4.6: Cross-sectional profile of 25 papillae collected from the AFM scans of *Loxosceles* silk described in *Figure 4.5*. The thick black line is the circular approximation made for the shape of the papillae so that the silk can be adapted to the roughness theory described in *Chapter 2.2.2* [23]

silk. Using $N = 7$ samples like the one seen in *Figure 4.5(a)*, this was accomplished. On the surface of the silk are nano-papillae and nano-fibrils that contribute to the roughness of the surface [9], [32]. Several important parameters determined by AFM were the RMS roughness: $2.496 \pm 0.56 \text{ nm}$, $\eta = 113.87 \pm 71.33 \text{ papillae}/\mu\text{m}^2$, average height of papillae: $8.89 \pm 1.63 \text{ nm}$, average width: $41.74 \pm 7.21 \text{ nm}$, average height of papillae-free surface: 9.11 nm , and $\sigma_s = 1.807 \text{ nm}$. These parameters allow us to now solve the asperity distribution function *Equation 2.5* and real contact area, *Equation 2.6*. Using the dimensions of the papillae, and estimating the average width as a chord of a sphere as shown in *Figure 4.6*. The radius of curvature of the papillae can be calculated as $R = 28.94 \text{ nm}$. The approximation of the papillae as being spherical loses information about the more Gaussian profile of the papillae, but for the purpose of evaluating the tangential force of the silk, this is an acceptable approximation. The Poisson ratio of *Loxoscles* silk is unknown, but can be approximated using other silks to be $\nu = 0.67$ [30].

The information gathered by way of tensile testing and AFM has allowed us to complete the *Kogut 2004* shear lap joint model for *Loxosceles* fibers, but not the tape [24]. Using the surface separation to be $d = 1\text{pm}$, the model predicts force to open a loop to be on the order of magnitude at $10^{-50}N$. At larger, more physical values of separation, MATLAB is unable to resolve the small values. The loop opening stress measured by *Koebly 2017* is 300 MPa which corresponds to a force of $100 \mu\text{N}$ using average dimensions of the silk [5].

Chapter 5

Conclusion

Prior research has shown that sacrificial bonds in polymers increase the material's toughness [10]–[12], and that the mechanisms of sacrificial bonds and load-cycling both work at all length scales as strain-cycling [5]. It has also been shown that, in the mechanics of elastic thin-films, there is a relationship between peel force and angle with respect to the substrate [13], [15]–[17]. To design a one-dimension thin-film mechanical metamaterial the properties of sacrificial bonds and load-cycling functioning in a thin-film system has been shown in this paper to function concurrently to increase and tune the toughness of the entire material.

To realize the design of this metamaterial, there must be a well defined geometry of the loop contact area as shown in *Figure 2.3*. This geometry was investigated by the preliminary tape tensile test experiment and verified by the rheometry experiment. These experiments found that there is no smooth function to describe the transition from peeling to lap shear joint mechanics. There is instead a critical angle at which there is a sharp transition between the delamination modes as shown in *Figure 4.2*. The critical angle was found to be: $145^\circ \leq \theta_{critical} \leq 147.5^\circ$. When $\theta_C < \theta_{critical}$ the loop fails according to the peeling mechanics described in *Chapter 2.2.1*. The force required to peel the loop open is directly proportional to the surface energy of the adhesive contact of the loop junction. This allowed us to calculate the surface energy

of Scotch®tape as $\gamma = 61 \pm 6.23 J/m^2$.

When $\theta_C > \theta_{critical}$, a lap shear joint delamination occurs. Parameters affecting the strength of this failure mode are the roughness, nominal contact area, Poisson ratio, and elastic modulus of the thin-film. Not all of these parameters have been obtained for the Scotch®tape. Due to the incomplete information, a complete model of the lap shear joint of this material is not yet possible. All of the necessary parameters have been determined for *Loxosceles* silk. The lap shear joint delamination mechanics model has been evaluated, but no reasonable results have come from it. The model predicts failure forces on the magnitude of $10^{-50} N$, when the loop opening force has been determined to be $100 \mu N$. This discrepancy is likely due to an incomplete model for this length scale. The model used was developed for macroscopic bulk materials in contact which is different from the silk because nano-scale forces were not accounted for. One assumption is for the model is that the asperities are non-interacting, but at the length scale of the nanopapillae, are likely interacting by way of van der Waals bonds. Other intermolecular forces could be involved and not accounted for in the model. Despite the model being void for the silk, it would likely be accurate for the Scotch®tape if all of the necessary parameters were obtained.

When engineering this one-dimensional thin-film mechanical metamaterial, the contact angle at which the loops are formed is the parameter that can be varied to tune the toughness of the entire system. When above the critical angle, more force is required to open the loops, and therefore the loops are stronger. Since the loops are the sacrificial bonds of the system, and each individual loop is stronger, the toughness of the entire system will increase. Another way to tune the toughness of the system that was not investigated in this paper is the adhesive of the contact area. *Loxosceles* silk likely uses van der Waals interactions to form the contact area but it is still unknown. The Scotch®tape uses a 3M™ pressure sensitive acrylic coating on a

single side of the thin UPVC film [31]. The capabilities of the mechanism for adhesion will effect the peeling mode delamination, but the lap shear joint is dependent on the roughness, and not the adhesive.

The *Loxosceles* spider naturally spins loops into its silk and forms the loops at $\theta_C = 157.44^\circ$ with $\sigma_{\theta_C} = 5.40^\circ$. This is $\approx 10^\circ$ above the critical angle. We can conclude that the *Loxosceles* loops are in the lap shear joint delamination mode. A cusp, that ensures lap shear joint mechanics, has formed on an individual loop is shown in *Figure 1.2*. It has been shown that the *Loxosceles* loop system increases the toughness of the silk by 30% [5]. Therefore we know the toughness increase caused by loops formed at $\theta_C = 157.44^\circ$. We would expect that the increase in toughness would be less when $\theta_C < \theta_{critical}$. More data needs to be collected to definitively determine this effect, and also determine if angles larger than 157.44° would increase the toughness by more that 30%.

Bibliography

- [1] X. Zheng, H. Lee, T. H. Weisgraber, et al. “Ultralight, ultrastiff mechanical metamaterials”. In: *Science* 344.6190 (June 2014), pp. 1373–1377. DOI: 10.1126/science.1252291.
- [2] Jae-Hwang Lee, Jonathan P. Singer, and Edwin L. Thomas. “Micro-/Nanostructured Mechanical Metamaterials”. In: *Advanced Materials* 24.36 (Aug. 2012), pp. 4782–4810. DOI: 10.1002/adma.201201644.
- [3] F. G. Omenetto and D. L. Kaplan. “New Opportunities for an Ancient Material”. In: *Science* 329.5991 (July 2010), pp. 528–531. DOI: 10.1126/science.1188936.
- [4] Hu Tao, Jason J. Amsden, Andrew C. Strikwerda, et al. “Metamaterial Silk Composites at Terahertz Frequencies”. In: *Advanced Materials* 22.32 (July 2010), pp. 3527–3531. DOI: 10.1002/adma.201000412.
- [5] S. R. Koebley, F. Vollrath, and H. C. Schniepp. “Toughness-enhancing metastructure in the recluse spider’s looped ribbon silk”. In: *Materials Horizons* 4.3 (2017), pp. 377–382. DOI: 10.1039/c6mh00473c.
- [6] Yang Guo, Zheng Chang, Bo Li, et al. “Functional gradient effects on the energy absorption of spider orb webs”. In: *Applied Physics Letters* 113.10 (2018), p. 103701. DOI: 10.1063/1.5039710. eprint: <https://doi.org/10.1063/1.5039710>. URL: <https://doi.org/10.1063/1.5039710>.
- [7] Nicola M. Pugno, Steven W. Cranford, and Markus J. Buehler. “Synergetic Material and Structure Optimization Yields Robust Spider Web Anchorages”. In: *Small* 9.16 (Apr. 2013), pp. 2747–2756. DOI: 10.1002/smll.201201343.
- [8] A. Meyer, N. M. Pugno, and S. W. Cranford. “Compliant threads maximize spider silk connection strength and toughness”. In: *Journal of The Royal Society Interface* 11.98 (July 2014), pp. 20140561–20140561. DOI: 10.1098/rsif.2014.0561.
- [9] Hannes C. Schniepp, Sean R. Koebley, and Fritz Vollrath. “Brown Recluse Spider’s Nanometer Scale Ribbons of Stiff Extensible Silk”. In: *Advanced Materials* 25.48 (Oct. 2013), pp. 7028–7032. DOI: 10.1002/adma.201302740.

- [10] Georg E. Fantner, Emin Oroudjev, Georg Schitter, et al. “Sacrificial Bonds and Hidden Length: Unraveling Molecular Mesostructures in Tough Materials”. In: *Biophysical Journal* 90.4 (Feb. 2006), pp. 1411–1418. DOI: 10.1529/biophysj.105.069344.
- [11] Xinxin Zhou, Baochun Guo, Liquan Zhang, et al. “Progress in bio-inspired sacrificial bonds in artificial polymeric materials”. In: *Chemical Society Reviews* 46.20 (2017), pp. 6301–6329. DOI: 10.1039/c7cs00276a.
- [12] Yichen Deng and Steven Cranford. “Tunable Toughness of Model Fibers with Bio-Inspired Progressive Uncoiling via Sacrificial Bonds and Hidden Length”. In: *Journal of Applied Mechanics* (Apr. 2018). DOI: 10.1115/1.4040646.
- [13] K. L. Mittal. “Adhesion Measurement of Thin Films”. In: *ElectroComponent Science and Technology* 3.1 (1976), pp. 21–42. DOI: 10.1155/apec.3.21.
- [14] K. Kendall. “Transition between Cohesive and Interfacial Failure in a Laminate”. In: *Proceedings of the Royal Society A: Mathematical, Physical and Engineering Sciences* 344.1637 (June 1975), pp. 287–302. DOI: 10.1098/rspa.1975.0102.
- [15] K Kendall. “Shrinkage and peel strength of adhesive joints”. In: *Journal of Physics D: Applied Physics* 6.15 (1973), p. 1782. URL: <http://stacks.iop.org/0022-3727/6/i=15/a=304>.
- [16] N. Aravas, K.-S. Kim, and M.J. Loukis. “On the mechanics of adhesion testing of flexible films”. In: *Materials Science and Engineering: A* 107 (1989). Proceedings of the Symposium on Interfacial Phenomena in Composites: Processing Characterization and Mechanical Properties, pp. 159–168. ISSN: 0921-5093. DOI: [https://doi.org/10.1016/0921-5093\(89\)90384-5](https://doi.org/10.1016/0921-5093(89)90384-5). URL: <http://www.sciencedirect.com/science/article/pii/0921509389903845>.
- [17] K Kendall. “Thin-film peeling-the elastic term”. In: *Journal of Physics D: Applied Physics* 8.13 (1975), p. 1449. URL: <http://stacks.iop.org/0022-3727/8/i=13/a=005>.
- [18] Kwang-Soo Kim, Jae-Seok Yoo, Yeong-Moo Yi, et al. “Failure mode and strength of uni-directional composite single lap bonded joints with different bonding methods”. In: *Composite Structures* 72.4 (Apr. 2006), pp. 477–485. DOI: 10.1016/j.compstruct.2005.01.023.
- [19] J. Katainen, M. Paajanen, E. Ahtola, et al. “Adhesion as an interplay between particle size and surface roughness”. In: *Journal of Colloid and Interface Science* 304.2 (Dec. 2006), pp. 524–529. DOI: 10.1016/j.jcis.2006.09.015.
- [20] J. A. Greenwood and J. B. P. Williamson. “Contact of Nominally Flat Surfaces”. In: *Proceedings of the Royal Society of London. Series A, Mathematical and Physical Sciences* 295.1442 (1966), pp. 300–319. ISSN: 00804630. URL: <http://www.jstor.org/stable/2415421>.

- [21] Bruno Zappone, Kenneth J. Rosenberg, and Jacob Israelachvili. “Role of nanometer roughness on the adhesion and friction of a rough polymer surface and a molecularly smooth mica surface”. In: *Tribology Letters* 26.3 (Jan. 2007), pp. 191–201. DOI: 10.1007/s11249-006-9172-y.
- [22] M. Bazrafshan, M.B. de Rooij, and D.J. Schipper. “The effect of adhesion and roughness on friction hysteresis loops”. In: *International Journal of Mechanical Sciences* 155 (May 2019), pp. 9–18. DOI: 10.1016/j.ijmecsci.2019.02.027.
- [23] D.B. Bogy W.R. Chang I. Etsion. “Adhesion Model for Metallic Rough Surfaces”. In: *Journal of Tribology* 110 (Jan. 1988), p. 50.
- [24] Lior Kogut and Izhak Etsion. “A Static Friction Model for Elastic-Plastic Contacting Rough Surfaces”. In: *Journal of Tribology* 126.1 (2004), p. 34. DOI: 10.1115/1.1609488.
- [25] M. Eriten, A.A. Polycarpou, and L.A. Bergman. “Physics-based modeling for fretting behavior of nominally flat rough surfaces”. In: *International Journal of Solids and Structures* 48.10 (May 2011), pp. 1436–1450. DOI: 10.1016/j.ijsolstr.2011.01.028.
- [26] B N J Persson, O Albohr, U Tartaglino, et al. “On the nature of surface roughness with application to contact mechanics, sealing, rubber friction and adhesion”. In: *Journal of Physics: Condensed Matter* 17.1 (Dec. 2004), R1–R62. DOI: 10.1088/0953-8984/17/1/r01.
- [27] Bettye L. Smith, Tilman E. Schäffer, Mario Viani, et al. “Molecular mechanistic origin of the toughness of natural adhesives, fibres and composites”. In: *Nature* 399.6738 (June 1999), pp. 761–763. DOI: 10.1038/21607.
- [28] Qijue Wang and Hannes C. Schniepp. “Strength of Recluse Spider’s Silk Originates from Nanofibrils”. In: *ACS Macro Letters* (Oct. 2018), pp. 1364–1370. DOI: 10.1021/acsmacrolett.8b00678.
- [29] J. A. Greenwood and J. H. Tripp. “The Contact of Two Nominally Flat Rough Surfaces”. In: *Proceedings of the Institution of Mechanical Engineers* 185.1 (June 1970), pp. 625–633. DOI: 10.1243/pime_proc_1970_185_069_02.
- [30] Kristie J. Koski, Paul Akhenblit, Keri McKiernan, et al. “Non-invasive determination of the complete elastic moduli of spider silks”. In: *Nature Materials* 12.3 (Jan. 2013), pp. 262–267. DOI: 10.1038/nmat3549.
- [31] 3M Scotch. *3M™ Scotch® Transparent Film Tape 600*. Tech. rep. 3M, Sept. 2009.
- [32] Qijue Wang and Hannes C. Schniepp. “Nanofibrils as Building Blocks of Silk Fibers: Critical Review of the Experimental Evidence”. In: *JOM* (Jan. 2019). DOI: 10.1007/s11837-019-03340-y.